JOURNAL OF PROPULSION AND POWER
Vol. 18, No. 5, September–October 2002

Assessment of Combustion Characteristics and Mechanism of Hydroxylammonium Nitrate-Based Liquid Monopropellant

Yi-Ping Chang* and Kenneth K. Kuo†
Pennsylvania State University, University Park, Pennsylvania 16802

The combustion characteristics and reaction mechanism of a HAN-based liquid monopropellant (HANGLY26, consisting of 60% HAN, 14% glycine, and 26% water by weight) were investigated. Combustion tests of liquid strands formed in test tubes were performed in an optically accessible strand burner. Fine-wire thermocouples were also installed in the strand to measure the temperature distribution of the reaction zone. The burning rate of HANGLY26 exhibited four burning rate regimes for pressures ranging from 1.5 to 18.2 MPa. No luminous flame was observed in any combustion tests. The temperatures of combustion products in the test tube were found to be near the water boiling points at pressures below 8.8 MPa. For pressures above 8.8 MPa, the product temperatures were found to be lower than the boiling points of water. Slope break points for burning rate vs pressure were found to coincide with those of concentration curves of recovered residues vs pressure. The observed slope breaks in burning rates are shown to be associated with the reaction mechanism changes between adjacent pressure regimes. Major species detected from the recovered liquid residues are nitrogen, nitric oxide, carbon dioxide, and formaldehyde. The pyrolysis of the fresh unburned liquid propellant was also studied. The results were compared with those of the recovered liquid residues.

Introduction

HYDROXYLAMMONIUM nitrate- (HAN-) based liquid monopropellants have been considered as potential candidates for the next-generation space propulsion applications because of their high density, low toxicity, and low freezing point.[1–3] In these propellants, HAN acts as the oxidizing component, and fuel-rich components are added to achieve higher energy release and higher flame temperature. Water is added to adjust the properties, such as viscosity and flame temperature. The chemical structure of HAN is shown in Fig. 1a.

HAN itself can be considered a monopropellant. The combustion characteristics and the reaction mechanism of HAN have been extensively studied by various researchers. Vosen[4] used a strand burner to study the apparent burning rate of an aqueous HAN solution with different concentrations. He found that the apparent burning rate first decreased with increasing pressure, then remained constant once the pressure exceed a threshold value of around 13 MPa. The reaction front was able to propagate through a rectangular tube with a 1.8×1.0 mm cross section. Therefore, the quenching distance of the HAN reaction is less than 1.0 mm, which was also explicitly stated in Vosen's later work.[5] Many researchers have taken fundamental approaches in the study of HAN reactions. For example, research investigations were conducted for solutions of low concentrations of hydroxylammonium ion (HA^+) combined with different concentrations of NO_3 (Refs. 6–8), pyrolysis of HAN in a nitrogen environment at 1 atm and at 129 or 139°C near its decomposition temperature,[9] an ignition and combustion study of HAN using accelerating rate calorimeter,[10] combustion of HAN and HAN-based liquid propellant XM46 under extremely high heating rate at atmospheric pressure,[11] confined rapid thermolysis studies of HAN,[12,13] and microexplosion studies associated with HAN-based liquid propellants.[14,15] It has been shown that HAN decomposition initiates in the condensed phase,[10,14] that the decomposition reaction exhibited autocatalytic behavior,[6–8,13] and that nitrous acid is an important reaction intermediate species.[9]

The HAN-based liquid propellant investigated in this study consists of 60% HAN, 14% glycine, and 26% water by weight. This propellant (HANGLY26 hereafter) was developed initially by Meinhardt et al.[16] The chemical structure of glycine is shown in Figs. 1b and 1c. Glycine is one of the amino acids that contain an acid ($-CO_2H$) and a base ($-NH_2$) within the same molecule. The proton transfer between acidic groups and basic groups could happen, forming the dipolar ion or internal salt,[17] as shown in Fig. 1c. A special name, "zwitterion," has been given to the internal salt of an amino acid. Johnson and Kang[18] conducted pyrolysis tests of glycine and other amino acids in a helium environment at a temperature range from 700 to 1000°C. Their study focused on the effect of amino acid structure on hydrogen cyanide (HCN) yield. It was found that the HCN yields of α-, β-, and γ-amino acids follow the order of $\gamma \gg \beta > \alpha$. The ratio between moles of HCN and amino nitrogen increased with increasing pyrolysis temperature. For some cases, this ratio could approach 100%. Simmonds et al.[19] studied the thermal decomposition of glycine and five other aliphatic monoamino–monocarboxylic acids at 500°C. They found that the common decomposition pathway for the amino acids studied is decarboxylation, generating carbon dioxide and amines. Amines would decompose further to give other decomposition species. Ratcliff et al.[20] extended the work of Simmonds et al.[19] and proposed primary and secondary decomposition pathways for α-amino acids. Chiavari and Galletti[21] pyrolyzed 19 α-amino acids at 600°C. Pyrograms and mass spectra data for these amino acids were reported. The formation of the pyrolysis fragments was explained by four decomposition pathways. Douda and Basiuk[22] studied the survivability of glycine and other amino acids under high-temperature and oxygen-free environments. The experiments were performed at different temperatures starting from 400°C with 100°C increments. It was found that glycine's survival rate was about 4% at 400°C and decreased to zero at 700°C.

The researchers of General Dynamics–Primex Aerospace Company conducted test firings using a flightlike thruster with HANGLY26 as the propellant.[16] The test runs were performed both in continuous mode and in pulse mode. The liquid propellant was ignited using a preheated catalytic bed. Reliable ignition and

Presented as Paper 2001-3272 at the 37th Joint Propulsion Conference and Exhibit, Salt Lake City, UT, 8–11 July 2001; received 27 July 2002; revision received 5 June 2002; accepted for publication 5 June 2002.

*Ph.D. Candidate, Department of Mechanical and Nuclear Engineering. Student Member AIAA.

†Distinguished Professor of Mechanical Engineering and Director of High Pressure Combustion Laboratory, Department of Mechanical and Nuclear Engineering. Fellow AIAA.

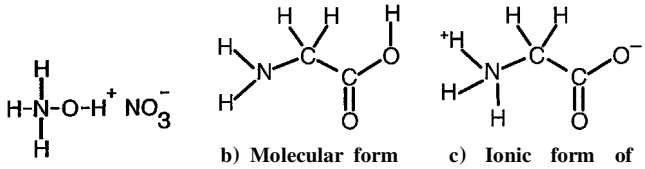

a) HAN b) Molecular form of glycine c) Ionic form of glycine

Fig. 1 Chemical structure of HAN and glycine.

clean, stable combustion were achieved. The specific impulse I_{sp} calculated from experiment data was in the range of 190–195 s. The exhaust plume was clean, and no carbonaceous residue was found in the catalytic bed. Fundamental strand burner tests of HANGLY26 were performed by Chang et al.[23] and compared with that of XM46 (60.8% HAN, 19.2% triethanolammonium nitrate, and 20% water by weight). The burning rate was found to be two orders of magnitude lower than that of XM46, but the flashback behavior of HANGLY26 was observed to be much less severe than that of XM46. Note that, although the weight percentages of HAN in these two propellants are nearly the same, the difference of burning rates is very significant. This prompted the authors' interest to further investigate the combustion characteristics and mechanism of HANGLY26 to gain a better understanding on the reason behind the difference.

In this study, the burning rate curve of HANGLY26 was extended beyond the pressure range reported earlier by Chang et al.[23] In addition, the temperature profiles of the combustion zone were measured at different pressures. The chemical analysis of the recovered liquid residues and the pyrolysis products of both fresh HANGLY26 and glycine were also performed to enhance the understanding of the reaction mechanism of this liquid propellant.

Experimental Approach

Liquid Propellant Strand Burner (LPSB)

A specially designed liquid propellant strand burner (LPSB), which contains an accurate liquid feeding system, was utilized to study the burning behavior of liquid monopropellants. The detailed description of the setup can be found elsewhere.[23,24]

All HANGLY26 combustion experiments were performed in LPSB. These experiments were conducted by filling liquid propellant into a glass tube (8-mm inner diameter). By the use of the glass tube, the monopropellant flame is confined in a nearly one-dimensional reaction zone. The combustion product gases were forced to accelerate in the vertical direction, resulting in a stretched reaction zone. This stretching effect was beneficial for observation of the combustion phenomena and was helpful in providing a comparison with one-dimensional model simulations.

The optically accessible windows of the LPSB allowed the visual observation of the whole combustion event and the usage of nonintrusive diagnostic techniques. Although the test chamber itself can sustain pressures up to 70 MPa, all liquid propellant tests conducted in this chamber were at pressures less than 35 MPa due to the limitations of the existing optically accessible windows.

Temperature Measurements in the Reaction Zone

A temperature profile across the burning surface of the propellant was measured using fine-wire thermocouples. S-type thermocouples were made of 25-μm pure platinum and 10% rhodium/platinum bare wires using a butt-welding technique under a microscope. Thermocouples were threaded through two diametrically opposite holes drilled on the tube wall, then sealed with beads of epoxy. The diametrically opposite holes were located at about 22 mm from the top of the test tube. After the epoxy cured, the location of the thermocouple was recorded.

An ice bath was utilized to provide the reference temperature point. It was found that the electronic reference points were more susceptible to electronic noise, which is a serious problem if instantaneous temperature measurements are required. The utilization of the ice bath, together with aluminum foil shielding on the outside of the thermocouple extension wire, greatly reduced the electronic noise from electromagnetic radiation and yielded very satisfactory signals. The thermocouple signal was amplified with a custom-made 100× amplifier to further increase the signal-to-noise ratio and then recorded using a data acquisition system for further analysis.

Chemical Analysis

A Shimadzu QP-5000 gas chromatograph/mass spectrometer (GC/MS), coupled with a Shimadzu PYR-4A high-temperature pyrolyzer, was used to identify and quantify the chemical species composition in the samples of interest. Two modes of operation were performed. One was to inject the sample directly into the injection port of the GC. The other was to put a small amount of sample in a platinum cup and drop it into the pyrolyzer at a preset temperature. The maximum temperature of the pyrolyzer is 800°C. The gas evolved either in the injection port or in the pyrolyzer was carried into the GC subsystem by helium, where different compounds in the gas were separated by the capillary column. The separated compounds passed through the transfer interface and went into the MS subsystem. The subsystem ionized and/or fragmented the compounds by electron beam and scanned through the specified mass-to-charge ratio (M/Z) range to determine the mass spectrum of the compound. The MS subsystem can scan the ions with M/Z between 10 and 700 at a maximum scanning rate of 6000 atomic mass units (amu)/s. The mass spectrum measured was compared with spectra of known substances by software to identify the species. Each compound was quantified by integrating the area under its chromatograph peak and comparing the area with the calibration constant obtained using the pure substance or samples with known concentrations.

Results and Discussion

Combustion Phenomena Observation

Combustion tests of HANGLY26 liquid propellant were conducted over the pressure range between 1.5 and 18.2 MPa. From the combustion phenomena observed, two pressure regimes (1.5–8.8 and 8.8–18.2 MPa) were identified, which corresponded to two distinct characteristics described hereafter.

Pressures Between 1.5 and 8.8 Megapascal

A typical image of the combustion event is shown in Fig. 2. No luminous flame was observed in this pressure regime. The reaction of the propellant formed a dark-cloud region on top of the regressing surface and translucent brown-colored gas beyond the dark-cloud region. From Fig. 2a, the region right beneath the dark cloud was translucent, but the image of the scale was somewhat distorted. This indicated the existence of gas bubbles. The bubbling phenomena at the regressing surface caused surface corrugation. Based on the visual observation of many test runs (not shown here), it is believed that the bubble size is larger for tests conducted at lower pressures. The dark-cloud region exhibited pulsating characteristics, that is, its length extended and retracted frequently, sometimes with translucent pockets formed within the dark-cloud region. The average height of the dark-cloud region was found to decrease as pressure was increased. The translucent pockets within the dark cloud would move upward to escape the dark-cloud region, resembling the upward motion of gas bubbles in the liquid. Occasionally, as shown in the three consecutive images taken 0.017 s apart in Figs. 2b–2d, droplets were observed in the translucent brown-colored gas region, located above the dark-cloud region. The existence of these droplets indicated that regions above the burning surface consisted of both gas- and liquid-phase material. Because of the continued combustion process in the dark-cloud region, energy was released, causing the gaseous products in the dark cloud to expand vertically. Thus, the length of the dark-cloud region changed with time. Also, some regions could have a lower amount of liquid droplets than others, as shown by the "gas pocket" in Fig. 2a. Because of the density difference, the lighter materials (called gas pockets) may subsequently escape the dark-cloud region, resulting in the retraction of its length.

Another observed interesting phenomenon is related to the recovery of liquid at the bottom of the test tube at the end of each test. The amount of recovered liquid residue decreases monotonically as the chamber pressure increases. As indicated in Fig. 3, the

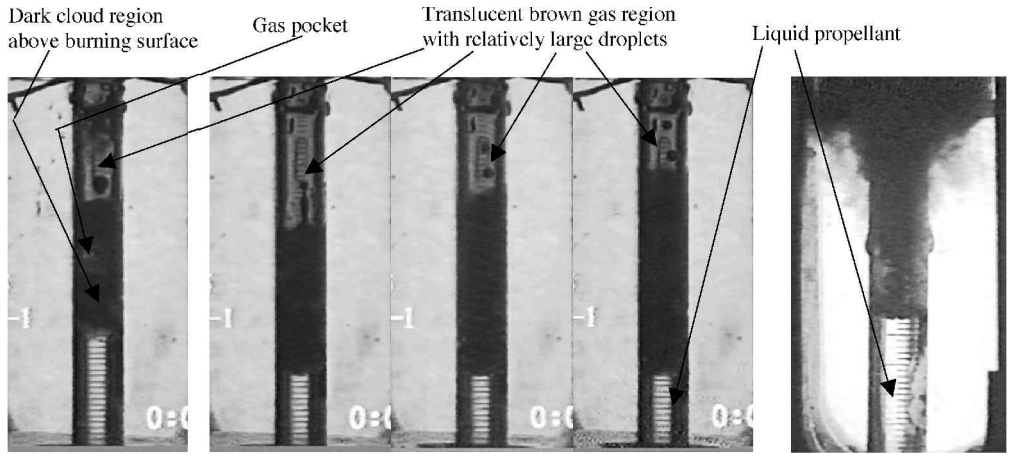

a) $t = 44.827$ s b) $t = 48.160$ s c) $t = 48.177$ s d) $t = 48.193$ s e) $t = 10.43$ s

Fig. 2 Test images of monopropellant HANGLY26 at a)–d) $P = 2.17$ and e) 11.8 MPa (grid size = 1 mm for both sets).

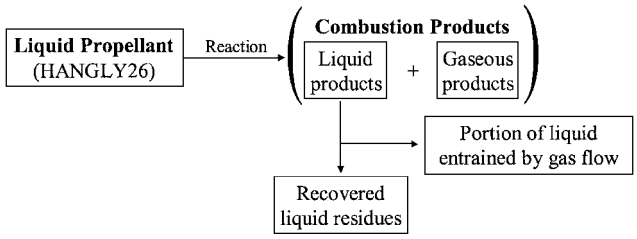

Fig. 3 Conservation of mass during combustion of the liquid propellant.

amount of liquid residue recovered depends on the liquid products generated at the burning surface and the portion entrained by the gaseous products.

Pressures Between 8.8 and 18.2 Megapascal

For tests conducted in this pressure range, the bubble size at the burning surface decreased to an indiscernible level, resulting in a flat reacting surface (see Fig. 2e). However, there was still no luminous flame. Unlike tests in the lower pressure range, no translucent brown gas was observed on top of the dark-cloud region; instead, the dark-cloud region filled up the whole tube above the reacting surface. Liquid sample could still be recovered after each test, although the amount was smaller as the pressure was increased.

That no luminous flame was observed in the pressure range studied prompts the question as to whether or not the adiabatic flame temperature of this particular propellant is high enough to generate luminosity. According to the calculations using the NASA Chemical Equilibrium with Applications (CEA) chemical equilibrium code, the adiabatic flame temperature of HANGLY26 is 1610 K, which is high enough to generate luminous flame. Furthermore, as shown in a later section, the product temperatures measured in the combustion tests were very low in comparison with the theoretical flame temperature. Therefore, we can conclude from both the visual observation and temperature measurements that the chemical energy of this propellant was not totally released in the tube tests because the second stage reaction was not triggered by any catalysts.

Pressure Dependency of Burning Rate

The burning rate was measured in static tests by filling the propellant into a 10-mm o.d. and 8-mm i.d. glass tube and allowing it to burn down into the tube. The burning rate as a function of pressure up to 18.2 MPa together with the data of a previous study[23] is shown in Fig. 4. As seen in Fig. 4, the burning rate can be fitted into four power-law regions: 1) $1.5 < P \leq 3.9$ MPa, 2) $3.9 < P \leq 8.8$ MPa, 3) $8.8 < P \leq 11.6$ MPa, and 4) $11.6 < P \leq 18.2$ MPa. The burning rate correlation as a function of chamber pressure is shown as follows:

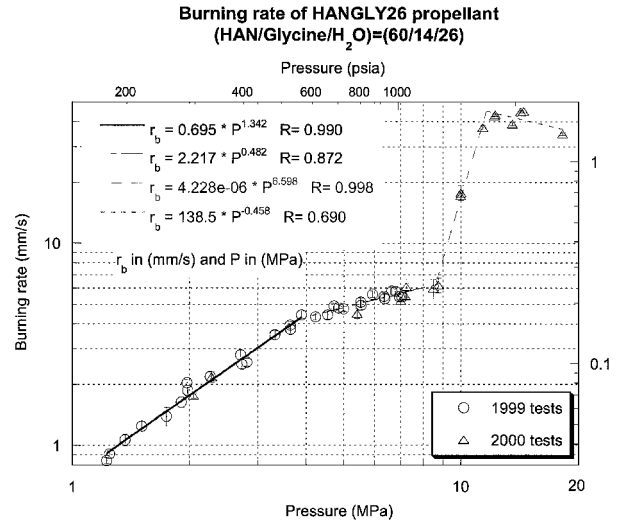

Fig. 4 Burning rate of HANGLY26 monopropellant as function of pressure.

$$
\begin{aligned}
r_b(\text{mm/s}) &= 0.695[P(\text{MPa})]^{1.342}, && 1.5 < P \leq 3.9 \text{ MPa} \\
r_b(\text{mm/s}) &= 2.217[P(\text{MPa})]^{0.482}, && 3.9 < P \leq 8.8 \text{ MPa} \\
r_b(\text{mm/s}) &= 4.228 \times 10^{-6}[P(\text{MPa})]^{6.598}, && 8.8 < P \leq 11.6 \text{ MPa} \\
r_b(\text{mm/s}) &= 138.5[P(\text{MPa})]^{-0.458}, && 11.6 < P \leq 18.2 \text{ MPa}
\end{aligned} \tag{1}
$$

The combustion of liquid monopropellant is a very complex phenomenon, involving not only the chemical reaction, but also the fluid dynamics, heat and mass transfer, etc. To understand the reason for the different burning rate trend at different pressure regimes, one needs to look at different aspects of the burning process. To achieve this goal, different diagnostic techniques are utilized to investigate various aspects of the combustion process. In the following sections, the results from different diagnostic techniques are discussed. After that, the underlying mechanism for the trend of the burning rate is discussed.

Temperature Distribution in the Reaction Zone

Temperature distributions inside the reaction zone were measured using 25-μm S-type thermocouples. Four typical temperature traces corresponding to the tests conducted at pressures equal to 2.1, 5.4,

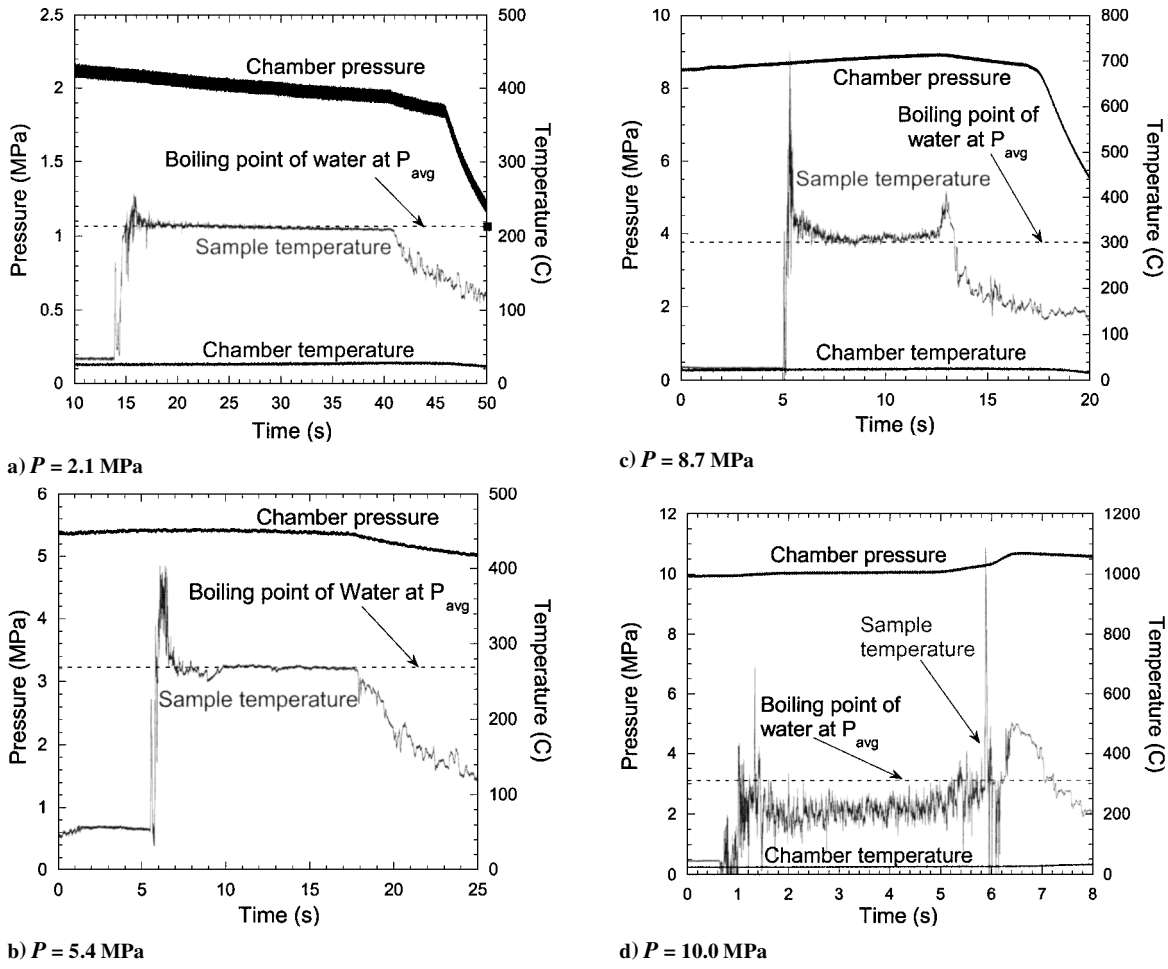

Fig. 5 Typical temperature and pressure traces at different chamber pressure ranges.

8.7, and 10.0 MPa are shown in Fig. 5. In Fig. 5a, the sample temperature increases abruptly as the burning surface approaches the bead location. The temperature reached a peak, then dropped down, and then leveled off. The temperature–time trace, shown in Fig. 5a, clearly indicates that thermocouple bead temperature corresponds to the boiling temperature of the water at the averaged chamber pressure for a significantly long period. The phase change process seems to dominate the temperature trace recorded by the thermocouple. The thermocouple traces at higher-pressure tests shown in Figs. 5b and 5c revealed the same type of behavior. The only difference is that near the end of the test of the case in Fig. 5c, the chemical reaction converting darker-colored material to translucent gaseous products could have released more thermal energy during this conversion period. This resulted in a temperature rise near the end of the test. For Fig. 5d, note the major difference between this case and all three other cases (Figs. 5a–5c). Instead of being at water's boiling point, the temperature trace of the combustion product for the case in Fig. 5d was below the boiling temperature. For the first three cases (pressure <8.8 MPa), there must be a significant amount of steam generated from the water boiling process because the temperature of products are so close to that of the boiling temperature of the water. For the case in Fig. 5d, less steam was evaporated from the water in the liquid propellant (LP) because the mixture temperature is below the boiling temperature of the water at the test chamber pressure condition. Corresponding to this situation, less energy from the combustion product is utilized to vaporize the water; hence, a higher percentage of energy feedback from the combustion zone above the surface can be used for pyrolyzing the HAN and glycine components at the burning LP surface at higher rates. This effect causes a significant increase in the pressure exponent for the third burning rate region with a pronounced slope break point at 8.8 MPa, as shown in Fig. 4. This high pressure-exponent region can, therefore, be considered to be associated with the steam suppression mechanism.

It is very unusual for a combustion system to have product temperatures so close to the water boiling point. As we pointed out in the discussion of Fig. 5c, the continued chemical reactions above the burning surface converted the dark cloud into translucent gas, causing a temperature rise near the end of the test. Obviously, the combustion front was just the first stage of the reaction and released only a portion of the chemical energy. The first-stage reaction zone exhibited a nearly isothermal domain, with a temperature on the order of 600 K. Therefore, the energy released during the first-stage combustion can be estimated as the sensible enthalpy change from 300 to 600 K if the product composition is known. The product composition was approximated by water plus the major pyrolysis products at 600 K. Thus, the sensible enthalpy change was estimated to be 664 kJ/(kilograms of propellant). If all of the water in the sample (26% by weight) went through the vaporization process at 8.7 MPa, the energy required would be 363 kJ/(kilograms of propellant). This corresponds to about 55% of the heat released in the first-stage reaction. This percentage is extraordinarily high for monopropellant combustion. Also, the percentage of energy required for water vaporization for the complete reaction, estimated using CEA code is about 21% of the total energy release from the initial temperature to the adiabatic flame temperature. This percentage is still a significant portion. In any case, this liquid monopropellant combustion process is somewhat peculiar in comparison with regular liquid fuels because it contains a considerable amount of water. The boiling processes of water, indeed, have a significant effect on the burning rate of the liquid propellant.

The fluctuation in the trace near the reacting front may represent the temperature variation inside the reaction zone. The thermocouple may be intermittently in contact with liquid and gaseous products, causing variations in the measured temperature–time traces. However, detailed examination of the temperature traces reveals that the variation can be as large as 489°C. The validity of temperature

nonuniformity in the reaction zone to such an extent is questionable. Furthermore, it was found that, for some cases, the temperature trace was momentarily lower than the propellant initial temperature after the reaction front reached the thermocouple bead. If we accept that the traces truly represent the temperature, it is hard to explain why the temperature could be lower than the propellant initial temperature. Therefore, it is believed that temperature nonuniformity was not the real source of the fluctuation in the temperature traces.

Another explanation for the fluctuation in the trace near the reacting front is believed to be the electrochemical effect between two parts of the thermocouple wire and the liquid in the reaction zone. It was observed that, when two separate wires (a 10% Rh/Pt wire and a Pt wire, which are the regular constituents of an S-type thermocouple) were purposely dipped into an unreacted HANGLY26 liquid propellant without touching each other, there was a voltage about 6 mV between two wires. However, when the bead of an S-type thermocouple was dipped into HANGLY26, it gave the correct output voltage corresponding to the LP temperature. In other words, the electrochemical effect was not detected when the liquid was not chemically reacting. This is because the electrical resistance for the current through the direct contact of the thermocouple junction is much lower than that through the ionic solution. The thermocouple junction essentially short-circuited the electrochemical current, causing the electrochemical voltage to be undetectable. However, in the neighborhood of the reaction front, there was a significant amount of liquid agitation due to the expansion of gas generated from either the evaporation process or chemical reaction. The liquid motion helped to move the ions around, which increased the effective ion diffusion velocity. The increased diffusion velocity corresponded to a decreased electrical resistance for the electrochemical current. When it is decreased to a level comparable to the direct contact resistance between the two parts of the thermocouple, the electrochemical effect becomes nonnegligible. In addition, the reaction could generate intermediate species and ions that have higher electrochemical potential. Thus, the contribution from electrochemical reaction to the overall current detected by the voltmeter cannot be neglected. Because the concentration of ions and intermediate species and the flow near the reacting front was not steady, the contribution from electrochemical effect was not constant either. Therefore, fluctuation of temperature traces was observed.

Chemical Analysis of the Residues Recovered from Combustion Tests

The liquid residue in the glass tube recovered from a given test was collected immediately after the combustion test for chemical analysis. The residues differ from the fresh LP in color. The former looks somewhat yellowish, and the latter is a clear liquid. The recovered samples, consisting of water and other dissolved reaction products, were analyzed using a Shimadzu QP-5000 GC/MS. Measured amounts of samples were injected into the injection port of GC system, whose temperature was set at 200°C. From the discussion in the preceding section, recall that the product temperature was in the range of 200–300°C. Because the injection port temperature is lower than the product temperature, the species detected should represent the original dissolved species in the liquid sample. In the chemical analysis, water was not measured because the variation of the dissolved species can shed more light on the physical understanding of this phenomenon. In addition, the water signal would be several orders of magnitude higher than those of other species and would cause the saturation of the sensor, which would result in significant wear of the equipment.

To show the difference between the liquid recovered from the tube tests and the fresh propellant, two chromatograms are shown in Fig. 6. Because the injection port temperature was set at 200°C, which is higher than the decomposition temperature of HAN at 145°C, the fresh propellant would decompose in the injection port and give pyrolysis products. However, the injection port is not designed for pyrolyzing purposes; therefore, the propellant may not be pyrolyzed in a very short time period. Because of the slower pyrolysis process, the peaks of major pyrolysis products, such as nitric oxide and carbon dioxide, appeared to be broadened with even double-peak phenomenon. Both the chromatograms of fresh propellant and recovered liquid from combustion tests exhibited the peaks of nitrogen, nitric oxide, carbon dioxide, nitrous oxide, and hydrogen cyanide. However, only the chromatograms of recovered liquid samples have the peaks of formaldehyde and formic acid. Furthermore, the chromatogram of residue has a much more noticeable peak of carbon dioxide than nitrous oxide, whereas that of fresh propellant has just the opposite. Based on the aforementioned differences, it can be concluded that if there is still some unburned propellant in the recovered liquid, the concentration is relatively low. This observation also implies that the material in the recovered liquid samples is quite different from that of fresh LP. Because the recovered residue showed a significant amount of gaseous chemical species, their presence in the residue is caused either by a condensed-phase reaction or by the absorption of gas-phase products into the LP during the combustion process.

In Figs. 7 and 8, the concentrations of the chemical species in the recovered liquid samples were plotted against the chamber pressure of various tests. For most chemical species analyzed, calibration constants were determined using high-purity ingredients. The errors of calibration constants are within 5%. However, the calibration constants for nitric oxide and hydrogen cyanide were estimated due to the unavailability of the high-concentration samples of these toxic

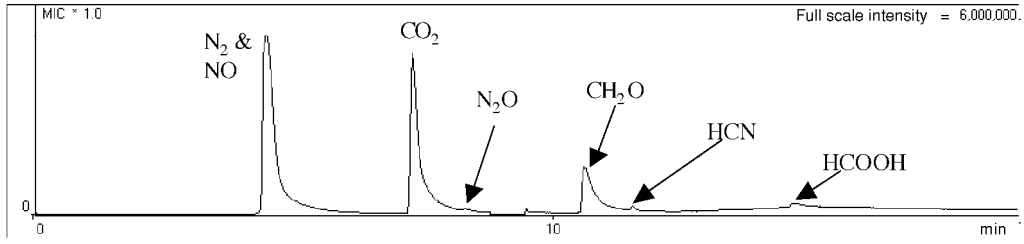

a) Multi-ion chromatogram of recovered liquid sample from test 113 conducted at P_{mean} = 2.28 MPa (331 psia)

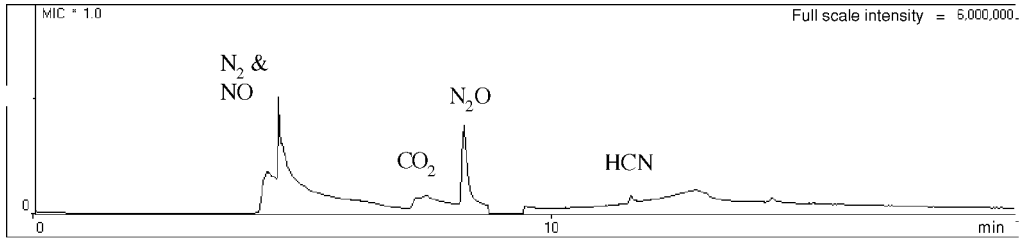

b) Multi-ion chromatogram of fresh HANGLY26 liquid monopropellant

Fig. 6 Comparison of chromatograms of recovered liquid samples with fresh propellant.

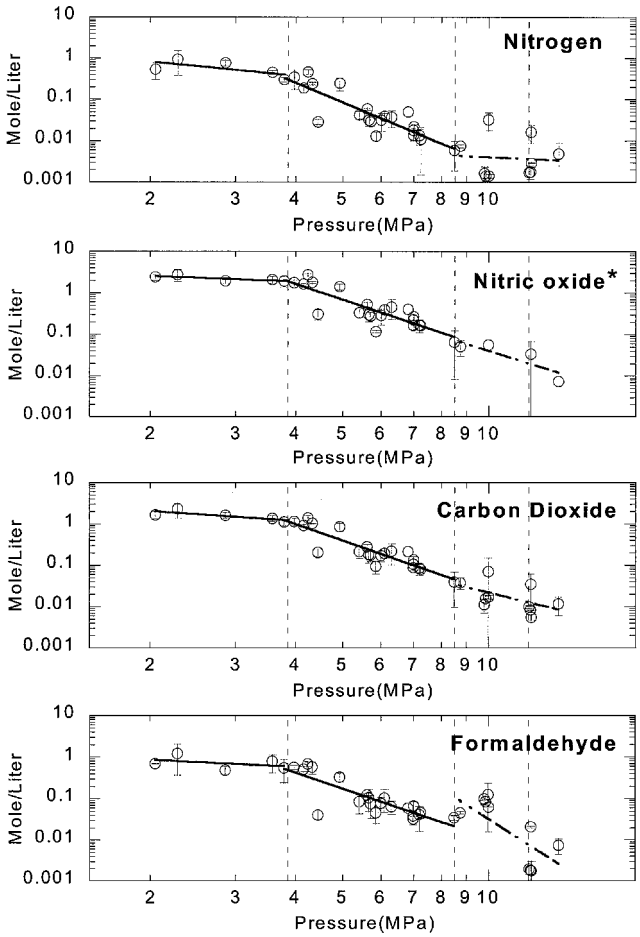

Fig. 7 Pressure dependency of species concentration of HANGLY26 propellant residue (*denotes species with estimated calibration constants, vertical - - - -, correspond to burning rate slope break points).

gases. The calibration constant of carbon monoxide was used in the estimate of the calibration constants for nitric oxide and hydrogen cyanide because of the similarity of the molecular structure between nitric oxide and carbon monoxide, as well as the similarity of covalence bonding between hydrogen cyanide and carbon monoxide (H—C≡N and C≡O). To obtain the general trend of concentration variation with pressure, it is reasonable to use the estimated calibration constants for these two species. The error bar of each data point, estimated by the standard deviation of the concentration measurements of the corresponding liquid residue, was also indicated in Figs. 7 and 8. For the majority of the recovered samples, the error bars for major species in Fig. 7 were less than 30% of the average measured concentration. Because of extremely small amounts of recovery, other recovered samples do not have satisfactory reproducibility. Usually, the procedure utilized in the residue analysis of this study was to rinse the microsyringe at least three times with distilled water, followed by three additional rinses with the recovered sample. After that, a measured amount of sample was drawn into the microsyringe. The purpose of the rinses with distilled water was to eliminate the previous sample trapped in the dead volume of the syringe. Similarly, the rinses with the sample eliminated the trapped distilled water. The rinses with the sample were necessary because the distilled water trapped in the dead volume could dilute the sample and affect the results. Thus, for an ideal test, the amount of sample needed was higher than what actually went into the GC/MS system. For cases with a smaller amount of recovered residues, fewer rinses with sample were conducted. However, the microsyringe was always rinsed with distilled water followed with at least one sample rinse. For very small amounts of recovered residues, the flushing of the injection syringe with the sample may not be sufficient to yield highly reproducible data. Although not all of the data points gave

Table 1 Intervals of the slopes in different pressure regime (95% confidence)

Species	Lower bound of m_2	Upper bound of m_2	Lower bound of m_1	Upper bound of m_1
Nitrogen	−6.11	−3.63	−3.41	1.15
Nitric oxide	−4.96	−2.84	−1.13	0.26
Carbon dioxide	−4.97	−3.20	−1.88	0.30
Formaldehyde	−5.10	−2.80	−2.77	1.64

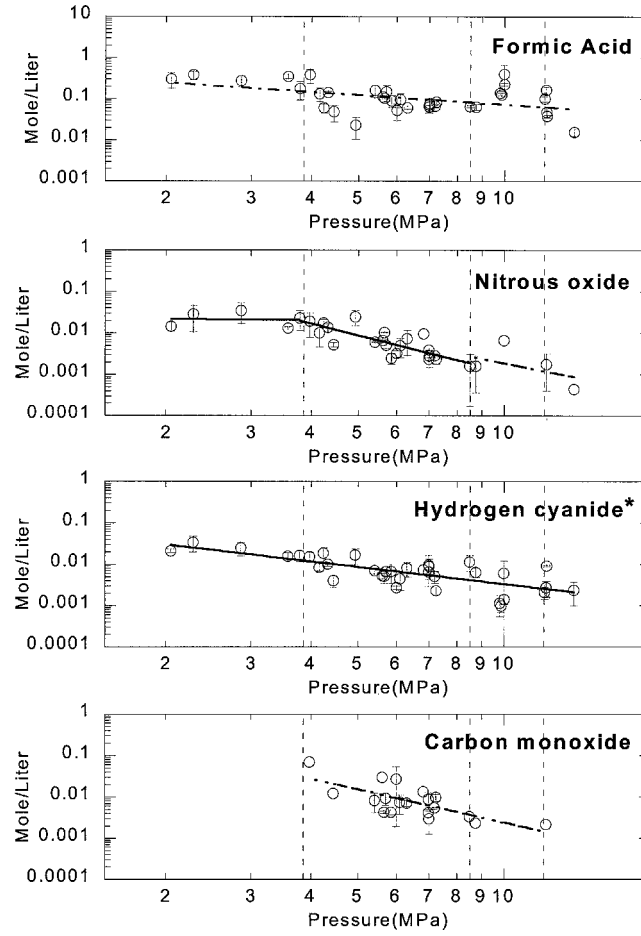

Fig. 8 Pressure dependency of species concentration of HANGLY26 propellant residue (*denotes species with estimated calibration constants).

very satisfactory reproducibility, they still gave a good representation of the overall trend.

In Figs. 7 and 8, the slope-breaking pressures of the burning rate curve are also indicated by vertical broken lines. These species evolved from recovered liquid samples and were grouped according to their concentration levels. Species with the concentration of about 1 mole/l are nitrogen, nitric oxide, carbon dioxide, and formaldehyde. Species with the concentration between 1 and 0.01 mole/l are formic acid, nitrous oxide, hydrogen cyanide, and carbon monoxide. Species with concentration lower than 0.01 mole/l are methanol, nitromethane, acetic acid, and acetonitrile. The data were curve fitted with power-law expressions at different pressure ranges. Although most of them were good fits, some of them were marginal due to the scattering of the data. For the latter cases, dash–dot lines were used to show the curve fit.

Note that in Fig. 7, the first slope break of the concentration vs pressure coincide with the slope-break pressure of the burning rate curve in Fig. 4. To verify that the concurrence is statistically meaningful, the 95% confidence intervals[25] of the slopes between 2.0 and 3.9 MPa (m_1) and between 3.9 and 8.8 MPa (m_2) are shown in Table 1. The change of slope would be statistically significant

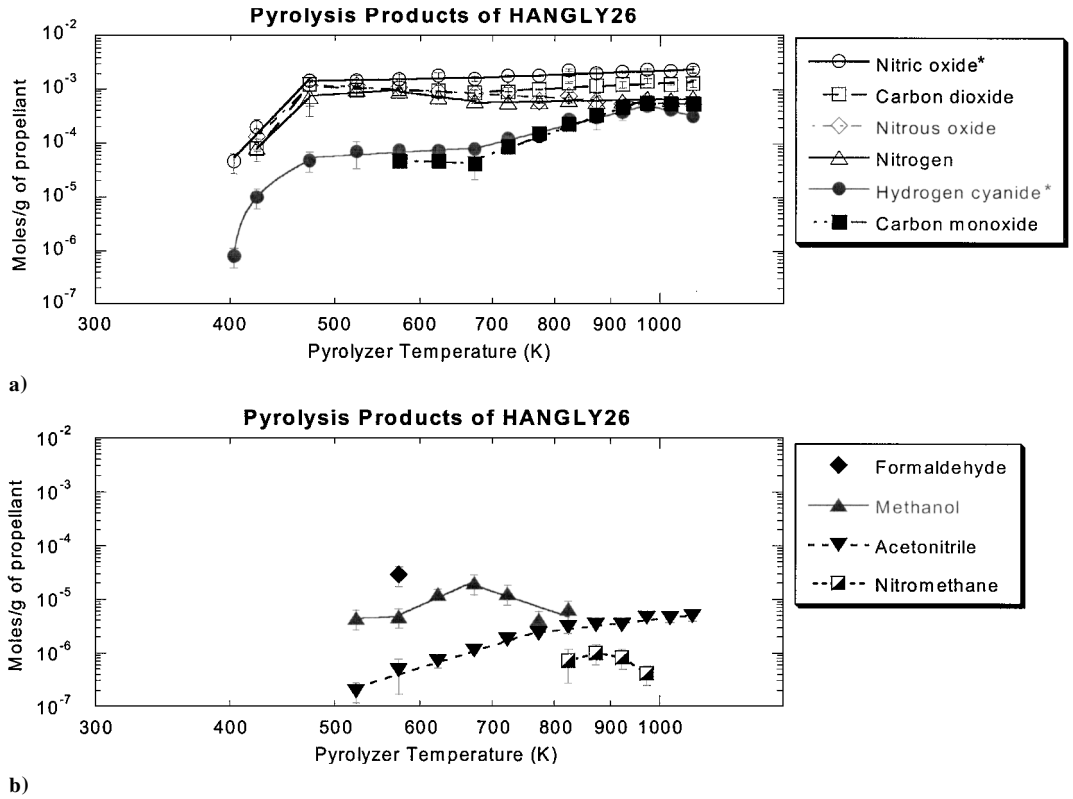

Fig. 9 Pyrolysis products of HANGLY26 as a function of pyrolyzer temperature (*denotes species with estimated calibration constants, HAN decomposition temperature ~ 418 K, glycine decomposition temperature ~ 475 K).

if these two confidence intervals did not overlap with each other. As shown in Table 1, there is no overlap between the confidence intervals of m_1 and m_2 for each species. Therefore, the difference of slopes at pressure equal to 3.9 MPa is statistically significant. This agreement in the slope break point between two separate sets of measurements strongly suggests the change of reaction mechanism from one pressure regime to the other regime.

Furthermore, the slopes of the major species concentration vs pressure plots in Fig. 7 for the pressure range below 3.9 MPa are quite similar, implying that they are nearly parallel curves. The same is true for the pressure range between 3.9 and 8.8 MPa. This further indicates that the concentration ratios of any two species in Fig. 7 are relatively constant at the first and second pressure regimes below 8.8 MPa.

Figure 8 shows the pressure dependency of concentrations of several minor species detected in the recovered liquid samples. Because of their relatively low concentrations, the signal-to-noise ratios for these species were lower, causing higher data scattering. Similarly, segments of power-law curve fit were performed on each of these species, and the curve fits with less confidence are shown in dash–dot lines. In Fig. 8, nitrous oxide was the only species that clearly exhibited a difference in the slope of the curve fit between different pressure regimes. The trend of nitrous oxide was very similar to those of the species in Fig. 7.

Pyrolysis Product Analysis of HANGLY26 and Glycine

To determine the type and amount of various chemical species generated from the LP, pyrolysis analysis was performed on HANGLY26 at temperatures above 403 K (in the neighborhood of HAN decomposition temperature of 418 K), and the results are shown in Fig. 9. To avoid data clustering, the results were split into Figs. 9a and 9b. Among the products, nitric oxide, carbon dioxide, nitrous oxide, and nitrogen are the ones having higher concentrations. For these species, the amount evolved increased rapidly as the pyrolyzer temperature increased from 403 to 473 K (130 to 200°C). Beyond 473 K, the amount of evolved nitric oxide increased slightly with increasing pyrolyzer temperature, whereas that of nitrous oxide decreased slightly. In Fig. 9a, hydrogen cyanide and carbon monoxide were less significant at lower temperatures. Hydrogen cyanide and carbon monoxide have almost followed the same curve, except that CO was not detected for pyrolyzer temperature below 573 K (300°C). In Fig. 9b, the result of formaldehyde, methanol, acetonitrile, and nitromethane are shown. Note that, with a 50-K increment of the this series of tests, formaldehyde was detected only at the pyrolyzer temperature of 573 K (300°C), and methanol exhibited a peak at 673 K (400°C). Apparently, the production of formaldehyde and methanol was most favorable near these temperatures. Compared with the results of residue analysis discussed earlier, the pyrolysis analysis of HANGLY26 did not reveal any new species, which is an indication that the absorption of the gaseous products into liquid residues may be negligible. From the results of HANGLY26 pyrolysis, there are several specific temperatures worth noting. In Fig. 9a, 473 K (200°C) and 673 K (400°C) were common slope-breaking points for the species plotted. Furthermore, 673 K (400°C) coincides with the peak location of the methanol curve.

Similarly, pyrolysis analysis was performed on aqueous glycine, and the results normalized to 1 g of glycine are shown in Fig. 10. The purpose of these tests is to understand the role of the fuel component during the pyrolysis of the liquid monopropellant. To ensure a higher accuracy of the sample amount, glycine was first dissolved into water with the weight percentage and density measured. The amount of glycine injected into the pyrolyzer was calculated as the product of the injection volume, density, and weight percentage. The pyrolysis results were divided into Figs. 10a and 10b for clarity. The traces of some species, such as carbon dioxide, ammonia, acetonitrile, and hydrogen cyanide, exhibited some slope breaks. The slope-breaking point of each species, however, did not coincide exactly with one another, as was the case of HANGLY26 pyrolysis analysis. The first slope-breaking points of these species were at about 623–673 K, which is about the same as the second slope break temperature of HANGLY26 at 673 K. Besides the aforementioned species, carbon monoxide, methane, propene, nitrous oxide, nitric oxide, nitrogen, ethane, and ethene were also evolved from the pyrolyzing glycine. Among them, methane, propene, and ethene started to evolve as the pyrolyzer temperature increased beyond 723 K, and ethane started

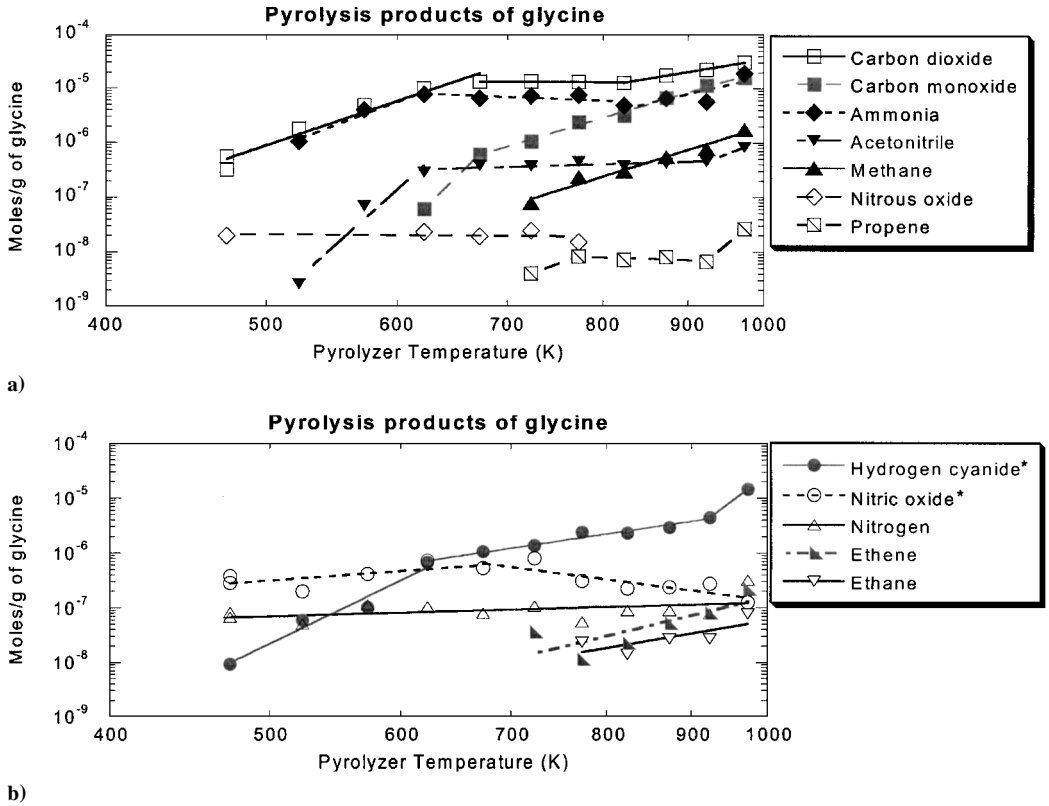

Fig. 10 Pyrolysis products of glycine at different pyrolyzer temperature (*denotes species with estimated calibration constants, glycine decomposition temperature ~ 475 K).

to evolve beyond 773 K. The detection of methane at temperature higher than 723 K suggested that methyl radical might be formed during the pyrolysis.[19] The amount of nitric oxide, nitrogen, and nitrous oxide species did not change appreciably with the pyrolyzer temperature.

The glycine decomposition mechanism was studied in detail by Ratcliff et al.[20] with several proposed decomposition pathways. The first primary decomposition pathway is decarboxylation by either unimolecular decomposition or heterolytic cleavage[19] for producing methylamine. The second primary decomposition pathway is the formation of dipeptide ($NH_2CH_2CONHCH_2COOH$) with water being released. With an additional dehydration reaction and ring closure, diketopiperazine ($C_4H_6N_2O_2$) is formed. The third primary decomposition pathway is the formation of a lactone (CH_2CO_2) releasing ammonia. The lactone further decomposes to give formaldehyde and carbon monoxide. In view of space limitations, the secondary reaction pathways are not included here, but are discussed in Ref. 26.

Controlling Mechanisms of the Burning Rate of HANGLY26

After reviewing all of the results from different diagnostic techniques, a further discussion on the controlling mechanisms of the burning rate of HANGLY26 monopropellant is provided in this section. From the visual observation, the temperature measurements of the reaction zone, and the recovery of the liquid residues, it was suggested that the products of HANGLY26 reaction in the strand-burning tests comprised both liquid and gaseous products. It is useful to first consider the mass conservation of the two-phase combustion products generated from the liquid propellant. Figure 3 indicates the formation of both the liquid and gaseous products. A portion of the liquid products was recovered, whereas the rest was entrained with the gas flow. Therefore, the amount of the recovered liquid residue depends on the amount of liquid-phase products generated and the portion entrained by the gas flow.

To further elucidate the effect of different parameters on the burning-rate pressure exponent, one can write down a simplified energy flux balance equation that shows the transition across the control volume from a cold, unburned station to the top of reacting surface[23]:

$$\rho_p r_b \left(\int_{T_i}^{T_s} C_p \, \mathrm{d}T + Y_w \Delta H_v \right) = \rho_p r_b Q_s + \dot{q}''_{\text{cond}} + \dot{q}''_{\text{rad}} \tag{2}$$

where ρ_p denotes propellant density, ΔH_v heat of vaporization of water, Y_w the mass fraction of water vapor produced by evaporation process, and Q_s the surface heat release per unit mass of propellant (considered positive for exothermic process) to form combustion products with all of the water in liquid state. Some portion of the water then evaporated into steam, which has a mass fraction of Y_w in the product mixture immediately above the burning surface. In Eq. 2, $\dot{q}''_{\text{cond}}$ denotes heat feedback by conduction and $\dot{q}''_{\text{rad}}$ radiative heat feedback. The conductive heat feedback can be further expressed as

$$\dot{q}''_{\text{cond}} = \lambda_{\text{gas/liquid}} \left. \frac{\partial T}{\partial x} \right|_{s,\text{product}}$$

Where $\lambda_{\text{gas/liquid}}$ is the thermal conductivity of the liquid and gaseous product mixture, s denotes the gradient evaluated at the reacting interface, and product denotes the gradients at the product side.

Because of a relatively low temperature on the product side, the radiative heat flux term can be neglected. Therefore, burning rate r_b can be expressed as

$$r_b = \frac{\lambda_{\text{gas/liquid}} (\partial T/\partial x)|_{s,\text{product}}}{\rho_p \left(\int_{T_i}^{T_s} C_p \, \mathrm{d}T + Y_w \Delta H_v - Q_s \right)} \tag{3}$$

Burning rate exponent n is the slope of r_b on the log–log plot and can, therefore, be written as

$$n \equiv \frac{\partial \ln r_b}{\partial \ln P} = \frac{\partial \ln \lambda_{\text{gas/liquid}}}{\partial \ln P} + \partial \ln \frac{[(\partial T/\partial x)|_{s,\text{product}}]}{\partial \ln P} - \frac{\partial \ln \left(\int_{T_i}^{T_s} C_p \, \mathrm{d}T + Y_w \Delta H_v - Q_s \right)}{\partial \ln P} \tag{4}$$

Thus, an abrupt change of any terms on the right-hand side of the equal sign can cause the abrupt change of the pressure exponent, contributing to the slope break on the burning rate plot.

At 3.9 MPa, there is a pronounced slope break in both the burning rate plot and the species concentration plot of the recovered residues. This implies that the change of pressure exponent of the burning rate curve was associated with the change of reaction mechanism. Furthermore, the decay of the concentration beyond 3.9 MPa for all of the major species (Fig. 7) suggests that the liquid-phase products decrease with increasing pressure.

The variation of the mass fraction of the liquid in the product mixture would change the thermal conductivity of the two-phase mixture ($\lambda_{\text{gas/liquid}}$). Generally speaking, the thermal conductivities of liquids are much higher than those of gases. In the current study, if the major pyrolysis products of HANGLY26 were used to estimate the thermal conductivity of the gaseous products, and saturated water were used to estimate the thermal conductivity of the liquid products, then it was found that the thermal conductivity of the liquid is roughly an order of magnitude higher than that of gaseous products. For a gas/liquid mixture, the upper bond of its thermal conductivity can be estimated as that of the liquid, and the lower bond the thermal conductivity corresponds to that of the gas. In other words, the thermal conductivity of gas/liquid mixture should approach that of the gas as the gas mass fraction approaches unity and approach that of the liquid as the liquid mass fraction approaches unity.

Test results suggest that a change of reaction mechanism from one pressure regime to the next one can cause the change of liquid mass fraction in the product mixture, which, in turn, induces the abrupt change of thermal conductivity of product mixture. This resulted in the slope break of pressure exponent n. As shown in Eq. (4), an abrupt change of the term associated with thermal conductivity would cause a change in the burning-rate exponent. To illustrate the feasibility of this postulation, the change of thermal conductivity needed to produce the slope break of the burning-rate plot was evaluated. At 3.9 MPa, the burning-rate slope changed from 1.342 to 0.482 with Δn equal to -0.860. From Fig. 7, it is reasonable to assume that $\lambda_{\text{gas/liquid}}$ at the pressure range between 2.0 and 3.9 MPa is relatively constant because the species concentrations of the liquid residues do not change much in this range. Therefore, $(\partial \ln \lambda_{\text{gas/liquid}})/(\partial \ln P)$ would be close to zero between 2.0 and 3.9 MPa. To produce a slope change of -0.860 caused by the change in the thermal conductivity from 3.9 to 8.8 MPa, the corresponding values of thermal conductivity λ_1 and λ_2 must be related by

$$\frac{\ln \lambda_2 - \ln \lambda_1}{\ln 8.8 - \ln 3.9} = -0.860$$

where λ_1 is the product thermal conductivity at 3.9 MPa and λ_2 at 8.8 MPa. From the preceding equation, we can determine the ratio of λ_1/λ_2 to be around 2.0. This implies that the variation of effective thermal conductivity of the gas/liquid mixture does not need to be one order of magnitude, associated with liquid/gas thermal conductivity ratio. Therefore, the slope change caused by the variation of thermal conductivity is probable.

As the pressure increased beyond 8.8 MPa, there was an abrupt increase in the pressure exponent of the burning-rate curve (Fig. 4). As demonstrated by the temperature traces, for pressures greater than 8.8 MPa, the boiling temperature of water is higher than the product temperature. This implies that there is a reduction of steam generation across the liquid/product interface. Therefore, less energy is required to vaporize the water in the LP. Thus, a higher percentage of energy feedback flux can be used to decompose the HAN and glycine compounds in the LP, causing the pressure exponent to increase significantly. This can also be seen from Eq. (3) for small values of Y_w.

The slope-breaking mechanism at 8.8 MPa can be examined by the energy flux equation. From Eq. (4), the change of water vaporization percentage contributes to the change of slope through the last term of the equation, which can be rearranged as follows:

$$-\frac{\partial \ln\left(\int_{T_i}^{T_s} C_p \, dT + Y_w \Delta H_v - Q_s\right)}{\partial \ln P} \approx -\frac{1}{\left(\int_{T_i}^{T_s} C_p \, dT + Y_w \Delta H_v - Q_s\right)} \times \left[\frac{\partial\left(\int_{T_i}^{T_s} C_p \, dT\right)}{\partial \ln P} + \frac{\partial (Y_w \Delta H_v)}{\partial \ln P} - \frac{\partial Q_s}{\partial \ln P}\right] \tag{5}$$

The contribution from the evaporation process is

$$-\frac{1}{\left(\int_{T_i}^{T_s} C_p \, dT + Y_w \Delta H_v - Q_s\right)} - \frac{\partial (Y_w \Delta H_v)}{\partial \ln P} = -\frac{(Y_w \Delta H_v)}{\left(\int_{T_i}^{T_s} C_p \, dT + Y_w \Delta H_v - Q_s\right)}\left[\frac{\partial \ln Y_w}{\partial \ln P} + \frac{\partial \ln \Delta H_v}{\partial \ln P}\right] \tag{6}$$

The terms in front of the braces [Eq. (5)] and square bracket [Eq. (6)] are all properties of the material or quantities resulting from natural processes; therefore, they should be continuous functions of pressure. However, the first derivative in the braces may exhibit some discontinuity. This would generate a slope increase in the burning rate plot. As shown in Fig. 7, the concentration of formaldehyde showed a sudden breakoff at 8.8 MPa from its decreasing trend at lower pressures. It is reasonable to assume that more hydrogen atoms were used to form formaldehyde than water vapor. Thus, the first term in the bracket can be a negative quantity after 8.8 MPa. This effect can, therefore, result in a pronounced slope break at 8.8 MPa.

Conclusions

Based on the experimental observations and analysis of measured data, several conclusions can be drawn:

1) Based on the strand burning test data at pressure range between 1.5 and 18.2 MPa, four burning rate regimes were identified for HANGLY26 LP. Below 8.8 MPa, the reaction of the propellant formed a dark-cloud region on top of the regressing surface and a subsequent translucent brown-colored gas-droplet region. For pressures greater than 8.8 MPa, no translucent brown gas region was observed on top of the dark-colored cloud region; instead, the dark-colored cloud filled up the whole tube above the reacting surface. Associated with the stronger blowing effect at high pressures, the translucent brown gas did not have a chance to form in the tube with limited length.

2) Various amounts of liquid residues were recovered from tests conducted at different pressures. The compositions of the residues were analyzed using a GC/MS system. Species in the recovered liquid residues were identified and their concentration quantified. The major species were found to be nitrogen, nitric oxide, carbon dioxide, and formaldehyde.

3) At the slope break point of 3.9 MPa, there is a noticeable change of dependency of species concentration on pressure detected from the recovered residues. This implies that the change of pressure exponent of the burning rate curve was due to the change of reaction mechanism. Comparing with the first regime, more gas-phase products are formed in the pressure regime between 3.9 and 8.8 MPa. Thus, the pressure exponent has a lower value in the second regime.

4) A pronounce slope break on burning rate plot was observed at 8.8 MPa. This slope break is believed to be caused by the reduction of the steam generation from the burning surface. For pressures lower than 8.8 MPa, the temperature of combustion products above the liquid/product interface was found to be the same as the boiling point of water. This indicates the dominance of water evaporation process at these pressures. Beyond 8.8 MPa, the product temperature was found to be lower than the boiling point of water. This implies that

less energy feedback from the reaction zone is required to vaporize the water in the LP. Thus, a higher percentage of energy feedback flux can be used to decompose the HAN and glycine compounds in the LP, causing the regression rate to increase significantly.

5) The pyrolysis products of fresh unburned HANGLY26 were analyzed in a GC/MS system coupled with pyrolyzer. Pyrolysis data indicated slope change of the yielded products with temperature at 473 and 673 K. Similar products species were found from the pyrolysis tests of fresh unburned HANGLY26 and recovered liquid residues from strand burner tests.

6) The pyrolysis products of glycine at different temperatures were analyzed. The results were in agreement with the literature. The detection of methane at temperature higher than 723 K suggested that methyl radical might be formed during the pyrolysis.

Acknowledgment

The major portion of the work has been supported by the NASA John H. Glenn Research Center at Lewis Field under the management of Brian D. Reed through Grant NAG3-2501 at the Pennsylvania State University (PSU). His interest and support are greatly appreciated. A portion of this work was funded by Primex Aerospace Company through Stacy Christofferson, E. J. Wucherer, and Dennis S. Meinhardt under Purchase Order M00886. Their support and encouragement are also gratefully acknowledged. The authors would also like to thank Baoqi Zhang of PSU for his participation in the early phase of burning rate measurements.

References

[1]Palaszewski, B., Ianoski, I. A., and Carrick, P., "Propellant Technologies: Far-Reaching Benefits for Aeronautical and Space-Vehicle Propulsion," *Journal of Propulsion and Power*, Vol. 14, No. 5, 1998, pp. 641–648.

[2]Sackheim, R. L., and Byers, D. C., "Status and Issues Related to In-Space Propulsion Systems," *Journal of Propulsion and Power*, Vol. 14, No. 5, 1998, pp. 669–675.

[3]Hurlbert, E., Applewhite, J., Nguyen, T., Reed, B., Zhang, B., and Wang, Y., "Nontoxic Orbital Maneuvering and Reaction Control Systems for Reusable Spacecraft," *Journal of Propulsion and Power*, Vol. 14, No. 5, 1998, pp. 676–687.

[4]Vosen, S. R., "Concentration and Pressure Effects on the Decomposition Rate of Aqueous Hydroxylammonium Nitrate Solutions," *Combustion Science and Technology*, Vol. 68, Nos. 4–6, 1989, pp. 85–99.

[5]Vosen, S. R., "Hydroxylammonium Nitrate-Based Liquid Propellant Combustion—Interpretation of Strand Burner Data and the Laminar Burning Velocity," *Combustion and Flame*, Vol. 82, Nos. 3–4, 1990, pp. 376–388.

[6]Pembridge, J. R., and Stedman, G., "Kinetics, Mechanism, and Stoicheiometry of the Oxidation of Hydroxylamine by Nitric Acid," *Journal of Chemistry Society, Dalton Transaction*, No. 11, 1979, pp. 1657–1663.

[7]Gowland, R. J., and Stedman, G., "A Novel Moving Boundary Reaction Involving Hydroxylamine and Nitric Acid," *Journal of the Chemical Society, Chemical Communications*, No. 18, 1983, pp. 1038, 1039.

[8]Stedman, G., Jones, E., and Garley, M. S., "Travelling Waves in Autocatalytic Oxidations by Nitric Acid," *Reaction Kinetics and Catalysis Letters*, Vol. 42, No. 2, 1990, pp. 395–399.

[9]Oxley, J. C., and Brower, K. R., "Thermal Decomposition of Hydroxylamine Nitrate," *Propulsion, Society of Photo-Optical Instrumentation Engineers*, Bellingham, WA, Vol. 872, Jan. 1988, pp. 63–70.

[10]Klein, N., "Ignition and Combustion of the HAN-Based Liquid Propellants," *Proceedings of the 27th JANNAF Combustion Subcommittee Meeting*, Vol. 1, Chemical Propulsion Information Agency, CPIA Pub. 557, Laurel, MD, 1990, pp. 443–450.

[11]Lee, Y. J., and Litzinger, T. A., "Combustion Chemistry of HAN, TEAN, and XM46," *Combustion Science and Technology*, Vol. 141, Nos. 1–6, 1999, pp. 19–36.

[12]Lee, H. S., and Thynell, S. T., "Confined Rapid Thermolysis/Fourier Transform Infrared Spectroscopy of Hydroxylammonium Nitrate," AIAA Paper 97-3232, July 1997.

[13]Thynell, S. T., and Kim, E. S., "The Effect of Pressure on the Thermal Decomposition Characteristics of Hydroxylammonium Nitrate," *Proceedings of the 35th JANNAF Combustion Subcommittee Meeting and 17th Propulsion System Hazards Subcommittee Meeting, Joint Sessions*, Chemical Propulsion Information Agency, CPIA Pub. 685, Laurel, MD, 1998, pp. 47–59.

[14]Zhu, D. L., and Law, C. K., "Aerothermochemical Studies of Energetic Liquid Materials: 1. Combustion of HAN-Based Liquid Gun Propellants Under Atmospheric Pressure," *Combustion and Flame*, Vol. 70, 1987, pp. 333–342.

[15]Call, C., Zhu, D. L., Law, C. K., and Deevi, S. C., "Combustion and Microexplosion of Han-Based Liquid Gun Propellants at Elevated Pressures," *Journal of Propulsion and Power*, Vol. 13, No. 3, 1997, pp. 448–450.

[16]Meinhardt, D., Brewster, G., Christofferson, S., and Wucherer, E. J., "Development and Testing of New, HAN-Based Monopropellants in Small Rocket Thrusters," AIAA Paper 98-4006, July 1998.

[17]Brown, W. H., *Introduction to Organic Chemistry*, 2nd ed., Sauders College Publishing, Orlando, FL, 1997, Chap. 18.

[18]Johnson, W. R., and Kang, J. C., "Mechanisms of Hydrogen Cyanide Formation from the Pyrolysis of Amino Acids and Related Compounds," *Journal of Organic Chemistry*, Vol. 36, No. 1, 1971, pp. 189–192.

[19]Simmonds, P. G., Medley, E. E., Ratcliff, M. A., and Shulman, G. P., "Thermal Decomposition of Aliphatic Monoamino-MonocarboxylicAcids," *Analytical Chemistry*, Vol. 44, No. 12, 1972, pp. 2060–2066.

[20]Ratcliff, M. A., Medley, E. E., and Simmonds, P. G., "Pyrolysis of Amino Acids. Mechanistic Considerations," *Journal of Organic Chemistry*, Vol. 39, No. 11, 1974, pp. 1481–1490.

[21]Chiavari, G., and Galletti, G. C., "Pyrolysis–Gas Chromatography/Mass Spectrometry of Amino Acids," *Journal of Analytical and Applied Pyrolysis*, Vol. 24, No. 2, 1992, pp. 123–137.

[22]Douda, J., and Basiuk, V. A., "Pyrolysis of Amino Acids: Recovery of Staring Materials and Yields of Condensation Products," *Journal of Analytical and Applied Pyrolysis*, Vol. 56, No. 1, 2000, pp. 113–121.

[23]Chang, Y.-P., Boyer, E., and Kuo, K. K., "Combustion Behavior and Flame Structure of XM46 Liquid Propellant," *Journal of Propulsion and Power*, Vol. 17, No. 4, 2001, pp. 800–808.

[24]Boyer, E., and Kuo, K. K., "High-Pressure Combustion Behavior of Nitromethane," AIAA Paper 99-2358, June 1999.

[25]Hines, W. W., and Montgomery, D. C., "Probability and Statistics in Engineering and Management Science," 3rd ed., Wiley, New York, 1990, Chap. 14.

[26]Chang, Y. P., "Combustion Behavior of HAN-Based Liquid Propellants," Ph.D. Dissertation, Mechanical and Nuclear Engineering Department, Pennsylvania State Univ., University Park, PA, Aug. 2002.